Astron. Astrophys. 330, 739–752 (1998)

ASTRONOMY
AND
ASTROPHYSICS

Meteor stream activity

VI. A survey of annual meteor activity by means of forward meteor scattering

I. Yrjölä[1] **and P. Jenniskens**[2]

[1] Jukolantie 16, FIN-45740 Kuusankoski, Finland
[2] NASA/Ames Research Center, Mail Stop 239-4, Moffett Field, CA 94035-1000, USA

Received 24 September 1996 / Accepted 12 August 1997

Abstract. The meteor activity of northern hemisphere streams was measured by means of radio forward meteor scatter. In 1994, there were 45 episodes of enhanced activity which were detected again in 1995, at both times on top of a continuous background of sporadic activity. Thirty of these enhancements were identified with known meteor streams by examining their daily variation of rates. For each stream, the radiant, the time of maximum, the duration, and the peak activity are given in units that allow direct comparison with prior results from visual observations. These results further refine models of the near-Earth dust environment and serve to characterise the properties of the current automatic meteor counting system for future use in the search for meteor outbursts.

Key words: meteors, meteoroids

1. Introduction

Present models of the near-Earth dust environment do not describe the significant flux variations of particles above 10^{-3} gram due to meteor streams (Lovell 1954, Hughes 1982, Steel 1993). Recent studies of major and minor nighttime meteor streams (e.g. Jenniskens 1994) make such possible, but have to be expanded to include daylight streams and meteor outbursts.

Daylight meteor streams can be monitored by counting reflections of radio waves from the ionised trails of meteors. Indeed, systematic surveys of meteor activity by means of backscattering radar have been performed by Hey & Stewart (1946), Prentice et al. (1947), Hawkins & Aspinall (1954), and Hawkins (1956), and have led to the detection of some strong daylight meteor showers (e.g. Lovell 1954, McKinley 1961, Hawkins 1964).

Meteor outbursts are transient enhancements of meteor rates over annual meteor stream activity (Jenniskens 1995). Of particular interest to us are the outbursts of streams that are due to debris of long period comets (Jenniskens 1997, Jenniskens et al. 1997). These outbursts are expected to occur only once or twice every 60 years, when the planets Jupiter and Saturn are at specific positions in their orbit and a trail of dust is brought in the path of the Earth. Hence, their detection calls for a continuous monitoring of meteor activity on a global scale. Radar systems are seldom used for this purpose because they are too expensive to operate on a continuous basis.

The technique of forward meteor scattering (MS) (Pierce 1938, Schilling 1993, Weitzen et al. 1993) is a good alternative and, in some respects, better than backscattering radar. This technique raises the altitude ceiling for detection of underdense trails and results in longer meteor reflection durations (Vogan & Cambell 1957). With equipment readily available and inexpensive to operate, many amateur meteor astronomers have used this technique to monitor the activity of major showers (e.g. Pilon 1984, de Meyere & Steyaert 1984, Mason 1986, Lehtoranta 1987, van Wassenhove 1987, Manley 1990, Artoos 1990, Morrow & Moore 1990, Tepliczky & Spanyi 1991, Kristensen 1991, Shimoda et al. 1993, Suzuki & Nakamura 1995, Richardson 1995, White 1995, and Bus 1995).

Most previous studies of meteor activity that use forward meteor scattering are fragmentary or only concerned with the diurnal and annual variation of mean monthly meteor rates in the context of establishing meteor burst radio links for data relay (e.g. Weitzen 1986, Weitzen & Ralston 1988). However, a more systematic and detailed study of meteor stream activity is possible from the theory of meteor stream observability in forward scatter, which was developed by Eshleman & Manning (1954), Hines (1955) and Moorcroft & Hines (1958) and applied to the Quadrantid meteor shower by Hines & Vogan (1957).

In this paper, we present meteor counts obtained by an automatic meteor counting system using forward meteor scattering during 1994 and 1995. We identify 45 temporary enhancements in meteor activity that are detected in both years. These are due to (complexes of) meteor streams. The data serve to further our understanding of annual meteor activity and are a baseline for the employment of this and other forward meteor scattering

Send offprint requests to: P. Jenniskens

systems in Global-MS-Net, a global network of amateur-run stations for the future detection of meteor outbursts.

2. Instrumental techniques

The present meteor counting system consists of a narrow band (15 kHz) FM receiver with central frequency f = 87.360 MHz, which is set to receive transmitted signals from a network of strong (5 kW, vertically polarized) commercial VHF transmitters at about 1300 km distance. The receiving antenna is a two-element Yagi with 4 dBd gain, aimed at the local horizon to azimuth 45^o (SW) in the direction of the main transmitters. This geometry favors the detection of bright meteors in large numbers.

2.1. Transmision

The dominant transmitters are located in Schönwalde (10.95E, 54.2N) and Heeslingen (9.33E, 53.2N) in northern Germany and are part of the Eurosignal paging network. The receiver is located at azimuth 138^o at a distance of 1190 and 1346 km respectively in Kuusankoski, Finland (26.4E, +60.9N), which puts the midpoint between receiver and transmitter at about (18E, +57N), over Gotland, Sweden. The potential scattering area is the overlap of the local horizons of the transmitters and receiver at the 80-110 km altitude layer in the atmosphere. Within the bandwidth of the receiver, 70% of signals are from the dominant transmitters at 87.3575 MHz. An additional 25% of signals have a frequency at 87.360 MHz, while 3% of signals have 5 other frequencies above 87.362 MHz. These are probably transmitters of the same network at different locations. A horizontally polarized antenna detected only 12% of the number of reflections registered by a vertical polarized antenna, most of which may be due to polarization rotation of overdense reflections.

2.2. Detection

The meteor reflection signals are sampled by measuring the signal to noise ratio at the receiver output as given by the DC voltage controlling the squelch gate. Meteor reflections that raise the DC voltage above a threshold level set at -122 dBm (dBm, deci Bels above one milli Watt), produce a binary (1 bit) signal to a 9 MHz Toshiba T-1000 SE laptop computer. During each observing interval, the computer logs four values:

1. The time of the start of the observing interval (in minutes since January 0.0 UT).
2. The total duration of triggered events (in minutes).
3. The number of triggered events.
4. The longest time that the signal was continuously above the detection level during the time interval (in seconds).

These data are saved in one hour intervals. Since February 13, 1995, 10-minute intervals are available also for later reference. Due to superposition of trails, the saturation limit of the system is reached at about 2800 counts/hour. Detection confidence drops for very short signals; all signals longer than 0.064 s are being recorded but none of duration less than 0.032 s. Nonspecular and fading trails near the threshold level are often counted more than once: a representative sample of 77 long duration echoes was counted a factor of 2.3 times too often. Also, the transmitters of the paging network are switched off for 2 seconds every 20 seconds, which affects the count (and recorded duration) of long reflections.

3. Methods of data reduction

The number of triggered events (the hourly count N) needs to be corrected for various forms of dead time and disturbances.

3.1. Dead time

The counting of an event prevents the subsequent registering of other events during the same period of time. If all signal strengths are hampered by the same signal duration ΔT, then the ordinary Geiger-counter correction applies:

$$N_c = N/(1 - N\Delta T) \quad (1)$$

However, the brighter meteors have longer lasting reflections that mask the reflections of fainter meteors. If an observed signal of given amplitude masks all signals of lesser amplitude for a time Δ T for any distribution of reflections, the correction is (Vogan & Campbell 1957):

$$N_c = 1/\Delta T \ \ ln(1/(1 - N\Delta T)) \quad (2)$$

where N is the observed hourly rate of reflections. This relation applies in first order when the stronger (overdense) signals are not frequent enough to significantly overlap and when destructive interference from signals reflected off other meteors causes no additional complications.

We have adopted Eq. 2 with ΔT = $< \Delta t_r >$ = 0.28 s. The correction is only significant for the major stream maxima. N_c will be called "N" in the rest of the paper.

3.2. Non-meteoric disturbances

Of 8760 hours in the year, down time for technical reasons was limited to about 72 hours in 1994 and 29 hours in 1995. In addition, there are some potential man-made interferences and some propagation phenomena that temporarily prevented meteor data collection or caused data distortion.

The system is relatively insensitive to local pulse type disturbances such as noise pulses from electric appliances and lightning. In the case of weak to moderate AC-power line type noise, no serious reduction on the meteor detection capability has been noticed. No effect was noticed of man-made and galactic noise background variations. The broad antenna pattern reduces galactic noise variation. Further suppression is achieved by on-purpose worsening the noise figure by some 4 dB with an attenuator, which reduces the bias from any noise floor variation. The receiver noise figure is 5 dB.

Maintaining detection threshold stability of this system is relatively easy because, on any FM receiver, the detection level

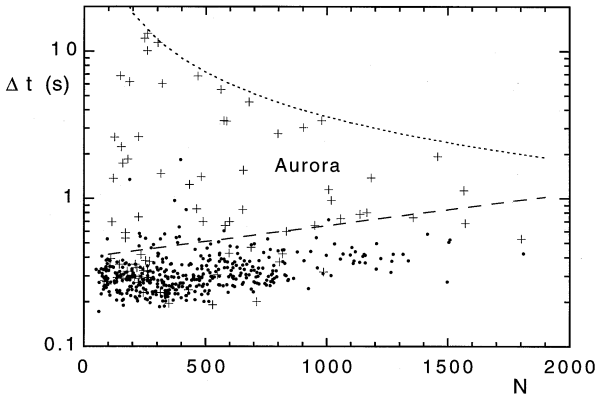

Fig. 1. The effect of aurora on the hourly count of reflections and the mean reflection duration. Data are shown during periods of aurora (+) and during periods of strong meteor stream activity (•).

drift is not caused by overall gain changes but receiver noise figure variations and noise amplifier/squelch gate gain/threshold drifts. The noise amplifier gain drift is compensated easily, since it occurs at a low gain audio frequency stage.

However, some abrupt changes in the daily counts are evident in the ratio of counts of 1995 versus 1994. Notably, there was a sudden decrease of counts by 20% on July 15, 1995, and another sudden decrease by 40% on February 13, 1995. The latter drop gradually adjusted back to former levels over a period until about March 7. These irregularities are tentatively ascribed to variations in the transmitted power of the combined network of German stations for which no records are available. Perhaps that unknown sensitivity variations of the detection system offer an alternative explanation. We have corrected the rates to the 1994 level by a simple multiplication factor where appropriate.

Of all propagation phenomena, only sporadic-E and aurora are observed, while line of sight, tropospheric, ionospheric and airplane scatter are being avoided by the selected geometry and setup.

Sporadic-E is not a serious problem at the high latitude of the observing site (+60N). When this event occurs, it is usually accompanied by slow fading and high signal levels, temporarily allowing continuous reception which can be easily recognized in the data during later analysis. Sporadic-E accounted for only about 51 hours of disturbance in the summer of 1994 and 33 hours in 1995.

Auroral propagation is the main cause of interference at the high latitude site of Kuusankoski. Auroral reflections on 87 MHz are received from an average azimuth of 100 degrees. They are possible only when the auroral oval extends far enough south over Sweden, to below latitude 62 degrees. The auroral interference can be recognized usually by their relatively long reflection duration. During data reduction, auroral spikes are removed from the data by deleting (and interpolating) all one hour counts with a total reflection duration (Δ t) in excess of a minimum value given by the dashed line in Fig. 1:

$$\log\Delta t(s) < -0.398 + 0.000215\ N \quad (3)$$

This algorithm excludes about 80% of all spikes due to aurora. Additional Auroral activity is removed by deleting those data that contain reflections lasting more than 60 seconds. That still leaves some remaining auroral spikes, which were removed by an algorithm that compares N with that of two adjacent hours and rejects the value if the ratio deviates by more than 50%.

In total, these procedures affected 2.5% of all data of 1994 (215 hours) and 1.1% of data in 1995 (95 hours). Fortunately, aurora does not normally persist long enough to interfer with the detection of the annual meteor streams discussed in this paper.

Unfortunately, these procedures do affect the detectability of meteor outbursts of short duration. Especially the final procedure may inadvertantly have deleted meteor outbursts that occurred during this two-year interval. In order to improve the situation, it was decided halfway through the experiment, to install a second receiver with a 12 element Yagi antenna, which was aimed North for back scatter signals of the Swedish auroral beacon SK4MPI on 144.960 MHz. The duration of the auroral signal on 144 MHz is stored, and the beacon keying cycle is verified by the software in order to prevent non-beacon originated signals being registered as aurora. Data is cross checked later with daily indexes of geomagnetic activity. These observations help identify auroral spikes in the meteor counts.

4. Results: sensitivity of the current system

4.1. Sensitivity of the system for sporadic meteors

The system's sensitivity for detecting meteors of a given magnitude can be estimated from the ratio of overdense and underdense echoes received. Underdense echoes are reflections from trails with a low electron density, where scattering occurs from individual electrons. Overdense echoes are reflections from trails with such high electron density that scattering occurs mainly at the outer skin of the trail.

By decreasing the sensitivity of the receiver, it is possible to detect the transition from underdense to overdense echoes by a change in slope of the number of detected reflections versus echo power, because overdense and underdense echoes have a different dependence of the echo power (P_e) on electron line density (α). For an underdense echo (McKinley 1961, Sugar 1964, Canon & Reed 1987):

$$P_e \sim \alpha^2 \quad (4)$$

while overdense echoes have:

$$P_e \sim \alpha^{0.5} \quad (5)$$

Such measurements were performed with two receiving systems of the same frequency and polarization, one of which was equipped with adjustable attenuation at the antenna RX input. High quality RF attenuators (Empire Devices AT 104) with 6 dB steps and two 2dB pads (MCL PAT-2) were used for the task. Counts were taken during the period Nov. 25 to Dec. 2, 1995, using 1 hour periods cycling randomly the attenuation in 2 dB steps. The unattenuated rates were measured by the second receiver with fixed sensitivity. The detection threshold was set at

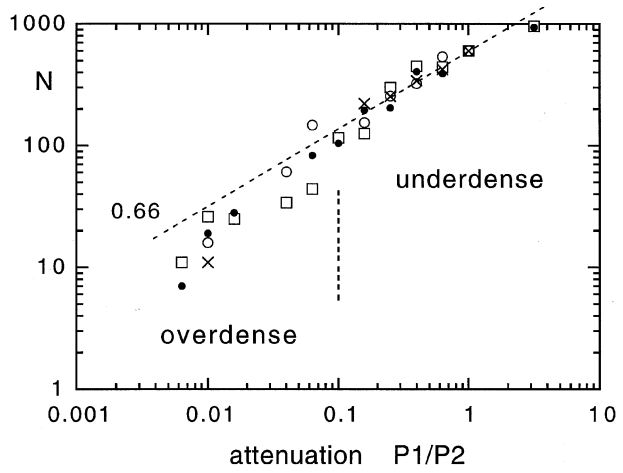

Fig. 2. The dependence of the daily count of reflections on the attenuation at the RX input.

-130 dBm, while other system parameters were: antenna gain 4 dBi, noise figure 2 dB, bandwidth 15 kHz (–6 dB) and frequency f = 87.36 MHz. The reader is reminded that the conversion from decibels (G) to power ratio is:

$$P_1/P_2 = 10^{G/10} \quad (6)$$

The results of the measurments are shown in Fig. 2, which plots the detected meteor rate (meteor reflections per day) versus the attenuation factor (P1/P2). Different symbols indicate data from different seasons in 1995. All are normalised at P1/P2 = 1.

The number of reflections N/N_c received versus the transmitted power (P), in this case controlled at the receiver side, is expected to vary as (McKinley 1961, Steyaert 1987):

$$N \sim P_e^{\epsilon} \quad (7)$$

assuming that the electron density is proportional to the luminosity of the meteor. With $m \sim -2.5log(\alpha)$, the exponent ϵ for underdense echoes is given by:

$$\epsilon = 0.5 \times (-2.5 \times log(\chi)) \quad (8)$$

and the exponent for overdense echoes is:

$$\epsilon = 2.0 \times (-2.5 \times log(\chi)) \quad (9)$$

where the magnitude distribution index (χ) is defined as (Jenniskens 1994):

$$\chi = n(m+1)/n(m) \quad (10)$$

Hence, for a typical magnitude distribution index of χ_s = 3.4 for sporadic meteors (Kresáková 1966), the expected exponents are ϵ = -0.66 and -2.66 respectively.

A dashed line in Fig. 2 shows the expected counts for underdense echoes only. Unfortunately, the transition from overdense to underdense is not sharp. This is partially due to intrinsic properties of the overdense meteor trains (Weitzen & Ralston 1988), but also because the slope is affected by multiple counts of long duration echoes. The turning point is at about P1/P2 = 0.05-0.2, which corresponds to a factor of $0.1^{-0.66} = 5\pm2$ higher rate (N) of underdense echoes (Eq. 7). This value compares well to the number of 19±5% of presumably overdense "bursts" counted while listening to the receiver output in sporadic nights. The corresponding shift in limiting magnitude follows from:

$$N \sim \chi^{(\Delta m)} \quad (11)$$

and is $\Delta m = +1.3\pm0.3$ magnitude. The meteor magnitude at the threshold from underdense to overdense is thought to correspond to magnitude m_v = +5.1 (Millman & McKinley 1956, Sugar 1964) and to a critical electron trail line density (α_c):

$$\alpha_c \sim f^2/81 = 9 \times 10^{13} \ \mathrm{e/m} \quad (12)$$

From this, the typical sporadic meteor captured at nominal performance of the system has a brightness $m = 5.1 + \Delta m = 6.4 \pm 0.3$ magnitude. The limiting magnitude of the system is about +0.9 magnitude higher than this, or more if the detection efficiency falls off gradually close to the detection limit. Hence, the limiting magnitude is 7.3±0.3 for sporadic meteors.

Table 1. Mean duration of reflections $< \Delta t_r >$ (after subtracting the contribution from sporadic meteors), from which the limiting magnitude of the radio meteors (Lm) is calculated as well as the mean radio meteor magnitude ($< m_r >$) for given geocentric entry velocity V_∞ and magnitude distribution index χ. These values may be compared to the mean visual magnitude ($< m_v >$), which was calculated from χ for a standard observer and standard sky conditions.

stream	$< \Delta t_r >$ s	Lm mag	$< m_r >$ mag	$< m_v >$ mag	V_∞ km/s	χ
Spo	0.28±0.02	+7.5	+6.7	+3.3	(43)	3.4
annual:						
Tau	0.45±0.08	(+9.1)	(+8.0)	+2.5	30	2.3
Gem	0.36±0.05	(+8.4)	(+7.4)	+2.8	36	2.6
Ari	0.30±0.03	(+8.5)	(+7.5)	+2.8	38	2.7
Boo	0.40±0.04	+7.4	+6.4	+2.7	43	2.5
Lyr	0.32±0.03	+6.9	+6.0	+2.8	49	2.7
Per	0.48±0.05	+5.2	+4.2	+2.7	61	2.5
eAq	0.42±0.03	+4.8	+3.9	+2.8	66	2.7
Ori	0.31±0.05	+5.0	+4.2	+3.1	67	3.1

4.2. Sensitivity for stream meteors

The limiting magnitude for stream meteors is dependent on the entry velocity (V_∞). One way to measure this velocity dependence is to examine the mean duration of the meteor reflections for various streams. The echo duration is a function of magnitude and V_∞, while the mean duration is also a function of magnitude distribution index χ and the limiting magnitude.

The mean reflection duration for the major streams was derived from plots of total reflection duration ($N \times \Delta t$) versus

count (N), after eliminating the sporadic background contribution ($N_s \times \Delta t_s$) according to:

$$\Delta t_r = (N\ \Delta t - N_s\ \Delta t_s)/(N - N_s) \quad (13)$$

Results are given in the second column of Table 1.

From radio echo theory (McKinley 1961), we calculated the limiting magnitude and mean magnitude of a meteor stream with $N \sim \chi^m$ that would result in the measured duration. We assumed an abrupt detection limit. For each magnitude (m), the line density (α) follows from (McKinley 1961):

$$m_r = 36.0 - 2.5\ log\ \alpha\ +\ 2.5\ log\ V_\infty(km/s) \quad (14)$$

The corresponding duration of overdense (m< 5.1) echoes is:

$$\Delta t^{ov}(s) = 6.6\ \times\ \alpha\ f^{-2}\ cos^{-2}(\phi)\ D^{-1} \quad (15)$$

where ϕ is half the angle between transmitter, meteor and receiver. The electron diffusion coefficient (D) is given by (from data in McKinley 1961):

$$\log D(m^2/s) = -0.24 + 0.0259\ V_\infty(km/s) \quad (16)$$

Underdense echoes (m > 5.1) have a different echo profile and a different dependence of echo duration on electron line density. After a sharp rise there is an exponential decay with a magnitude independent echo decay time (τ_u) defined as the time after which the signal has decayed to e^{-2} times the peak power (McKinley 1961):

$$\tau_u(s) = 5.7 \times 10^{14}\ f^{-2}\ cos^{-2}(\phi)\ \ D^{-1} \quad (17)$$

The echo duration (Δt^{un}) is a function of the peak power (P) and the power threshold level (P_t). With P$\sim \alpha^2$, we have for all $\alpha_c > \alpha > \alpha_t$:

$$\Delta t^{un} =\ \tau_u\ ln(\alpha/\alpha_t) \quad (18)$$

The threshold line density follows from (Eq. 14):

$$\mathrm{Lm}\ =\ 36.0\ -\ 2.5\ log\ \alpha_t\ +\ 2.5\ log\ V_\infty \quad (19)$$

The result for sporadic meteors, with Lm = 7.3, $< V_\infty >$ = 43 km/s, and χ = 3.4, is $< \Delta t_r >$ = 0.287 s, which is in good agreement with the measured value of $< \Delta t_r >$ = 0.28±0.02 s. We now use these equations to find the limiting magnitude Lm for which the model gives the measured mean duration of stream meteors. The results are given in the second and third column of Table 1 and plotted by open symbols in Fig. 3. In Table 1, these results are compared to the mean visual magnitude $< m_v >$.

Surprisingly, we do not find a solution for streams with a low entry velocity $V_\infty < 40$ km/s. The measured echoes should have been longer. Indeed, we confirm that the average burst duration of underdense echoes goes down with increasing relative threshold faster than predicted in the classical model (Ralston et al. 1993). If we adopt a relation such as:

$$\Delta t^{un} = \tau_u \times exp((5.1 - m)/3) \quad (20)$$

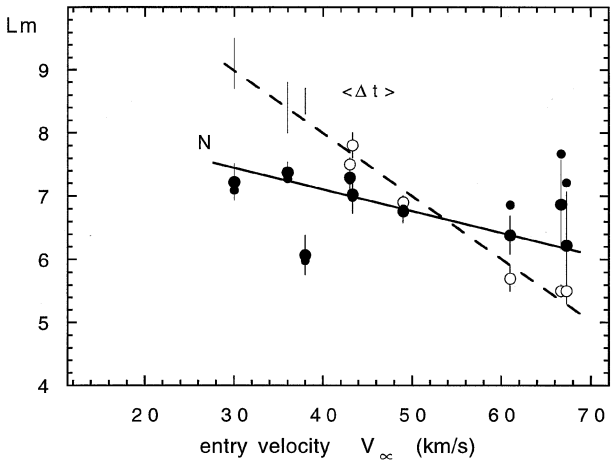

Fig. 3. Limiting magnitude (Lm) for meteors of given entry velocity (V_∞), derived from the measured mean reflection duration (open symbols) in Sect. 4.2 and derived from the recorded rate of reflections (closed symbols) in Sect. 5.2.

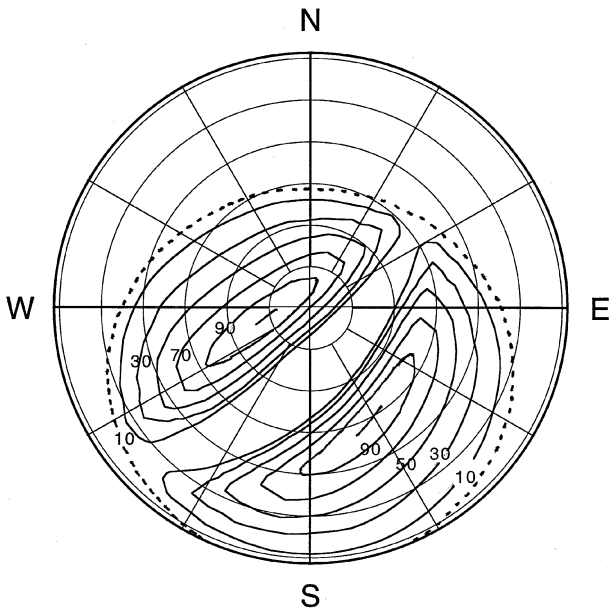

Fig. 4. Observability function for meteors with a radiant at given hour angle and declination for a receiver-transmitter azimuth of 45 degree, a distance of 1300 km, and a midpoint at latitude 57 N - after Hines (1955) and Moorcroft & Hines (1958).

then the result for the high velocity streams are still about the same and the results for the low velocity streams become the values that are given between brackets in Table 1.

Clearly, this simple model suggests that the limiting magnitude of our system is a strong function of entry velocity (Fig. 3). However, we find similar ratio's of overdense and underdense echoes for some of the major streams and there is no indication that the slow streams are so much better detected. We will come back to this in Sect. 5.2, when discussing the recorded meteor stream activity.

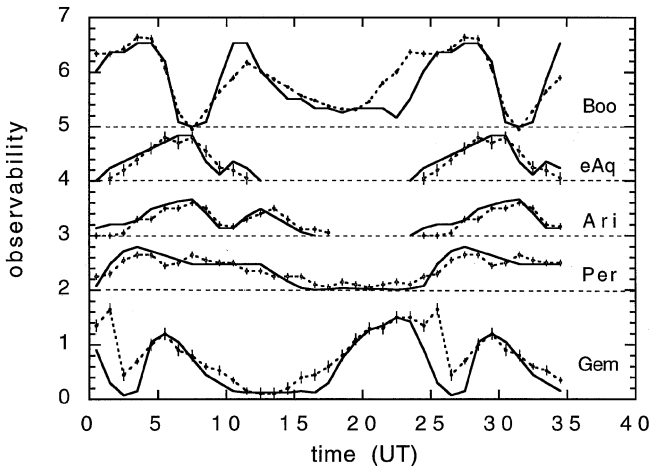

Fig. 5. Observability of the major showers. Solid lines are derived from Fig. 4 and compared to normalised observed radio rates relative to visual zenith hourly rates (points, dashed lines).

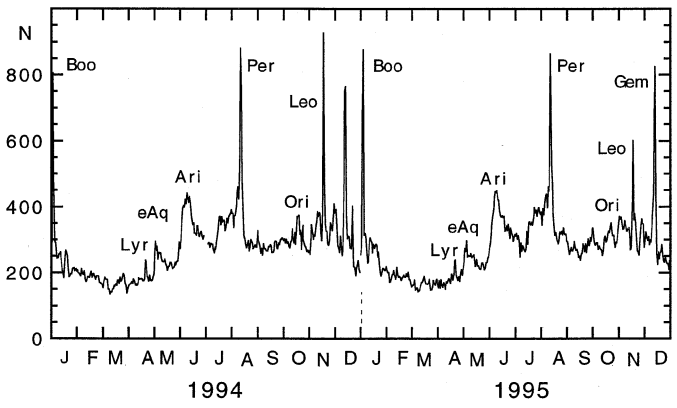

Fig. 6. Daily variation of counts in 1994 (left) and 1995 (right). The total daily mean hourly count of meteor reflections (N) is given as a function of date in the year. Some of the major showers are indicated.

4.3. Sensitivity as a function of radiant position

The system response to meteor streams is a function of radiant elevation and the relative position of the radiant with respect to the direction from receiver to transmitter (Eshleman & Manning 1954, Hines 1955). This "observability function" is a combination of four effects. Most important is the radiant elevation (h_r) dilution, which is a geometric effect leading to a rate dependence of $\sim sin(h_r)^{-1}$. In addition, there are the effects from the fraction of trails of given orientation that have favorable observing geometry, the geometric area seen by both receiver and transmitter, and the illumination function which is a combination of antenna patterns for receiver and transmitter.

The observability function for a receiver-to-transmitter direction of azimuth 45 degree, a distance of 1300 km, and a midpoint at latitude 57 N, was calculated from the observability function published by Moorecroft & Hines (1958) using a procedure given in Hines (1955). This function is derived assuming horizontally polarized links, but is very similar for our case of vertically polarized observations. This is because the common scattering area far from the receiver-transmitter line, which does not provide observable geometry in the horizontal case, is only a small area. Although the receiving antenna pattern has a Half-Power-Beam-Width = $\pm 70^o$ horizontally and $+35^o$ vertically, the potential scattering area covers only a range of $\pm 52^o$ in azimuth and up to 12^o in elevation at the receiving station due to the large distance of the transmitters.

Fig. 4 shows the observability function in terms of hour angle and polar distance of the radiant position. The observability function of a given stream can be easily read from this diagram, because in one day the radiant moves at a constant rate along a circle of constant declination around the north celestrial pole, following the circles in the diagram (Forsyth et al. 1955).

Figs. 5 compare the observed diurnal variation of rates of some major showers with that predicted from Fig. 4, given the meteor activity curves derived in Jenniskens (1994). There is good agreement and no systematic deviation that warrants an adjustment of the function of Fig. 4, except perhaps that the minimum is not as deep, which can be due to the geographical spread of transmitting stations and the long 1-hour sampling interval.

5. Results: meteor rates

The system in its current configuration was initiated in August of 1993 and has been in continuous operation since September of that year. Of all stored parameters, the meteor count N showed best signal-to-noise ratio and was selected to be used for further analysis. Results are shown in Figs. 6 to 8.

Fig. 6 shows the total daily count of meteors in the period between January 1, 1994, until December 31, 1995. The peaks are due to the major meteor streams. All but one (Leonids) are detected in much the same way in both years. These are the annual meteor streams. The Leonids had a meteor outburst in both years, but the event in 1994 was much stronger than in 1995, causing a significant variation in rates.

Our system is found to be significantly more stable and more sensitive than conventional field strength based observing systems. The squelch sampling technique suppresses noise effectively, improving the sensitivity by about 45%. Not only did we detect the same streams in both years, we also obtained counts at a given date in 1995 similar to that in 1994. Hence, the typical drift in the receiver noise figure is less than a few tenths of a dB.

Fig. 7 shows an example of 10-minute counts obtained over a period of seven days during the Perseids of 1995. The counts rise and fall daily, reflecting the changing position of the apex of the Earth, the rising and setting of meteor stream radiants, and the changing observability. Typically, the higher the apex (for sporadic meteors) or the radiant point (for meteor streams) in the observer's sky, the higher the rate. Hence, the lowest echo rates occur in the late afternoon, the highest in the early morning hours.

Fig. 8 depicts the data in a manner that show better the daily variation of meteor stream rates, by plotting the meteor rates at

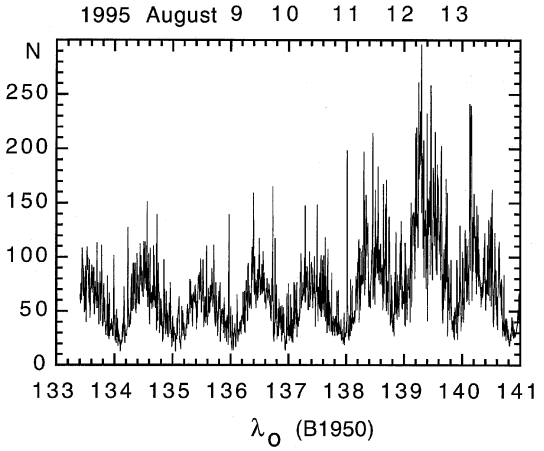

Fig. 7. Example of raw meteor counts in 10-minute intervals recorded over a period of seven days in August of 1995. The Perseid shower is responsible for increased rates around solar longitude 139.

a given time of the day as a function of the day in the year. Fig. 8 shows the hourly count over the same time interval as Fig. 6, but for the single hour starting at 11h, 17h, 23h and 05h UT. The variation of meteor rates in these graphs is a good depiction of the meteor stream activity curves, because the observability of a given meteor stream does not vary significantly over a period of a few days for a given time of day. From these diagrams, we will now examine the sporadic activity (Sect. 5.1) and the presence of meteor streams (Sect. 5.2).

5.1. Sporadic activity

The meteor streams are found on top of a continuous background of sporadic meteors. Contrary to previous studies, our data allow us to define the level of sporadic activity underlaying the temporary enhancements of meteor rates by placing a baseline assuming the functional form:

$$N(H, \lambda_\odot) =< N_{\rm spo} > (H) - \Delta N_{\rm spo}(H)\ cos(\lambda_\odot) \qquad (21)$$

where $< N_{\rm spo} >$ is the mean daily sporadic hourly count at the Summer solstice on June 21 and $\Delta N_{\rm spo}$ is the yearly amplitude due to the seasonal variation at a given local time of the day (H). $\lambda_\odot$ is the solar longitude, which is given throughout the paper in epoch 1950. This form assumes that any concentration of reflections along the ecliptic plane is due to a meteor stream. In that case, the only variation in rates expected at a given time of the day is due to the varying altitude of the ecliptic plane over the year. On the northern hemisphere, rates are expected to peak in the Autumnal Equinox (about September 21) and to be lowest during the Vernal Equinox (March 21).

Placing the baseline is not trivial, however, because there are some widely dispersed and unknown minor streams in the data. The placement of these curves is mainly determined by assuming that minor stream activity is negligible in March and April (solar longitude 0-30) and in late August and September (solar longitude 150-180). Some typical curves are shown as dashed lines in Fig. 8.

Results for $< N_{\rm spo} >$ and $\Delta N_{\rm spo}$ are summarized in Fig. 9. We find that the diurnal variation in $< N_{\rm spo} >$ is well described by a model with radiant positions homogeneously distributed on the sky, for which the expected behavior is (Schiaparelli 1866, Lovell 1954 p. 96):

$$< N_{\rm spo} >= K\ (1 + \mu\ cos(\phi)\ sin(H)(1 - 0.25\ sin^2\epsilon')) \qquad (22)$$

where ϕ is the observer's latitude, ϵ' the obliquity of the ecliptic (ϵ' = 23 degree), and $\mu = V_E/V_H$, where V_H is the mean heliocentric velocity of the meteors. The dashed curve in the upper graph of Fig. 9 shows a solution with V_H = 36 km/s and K = 190, which gives a good fit to the data, except for somewhat higher rates in the early morning hours which may represent unrecognized minor streams. A mean $< V_H >$ = 36 km/s corresponds to $< V_\infty >$ = 41.2 km/s, close to the measured mean sporadic velocity of 43 km/s (McKinley 1961).

Finally, we find that the seasonal amplitude of sporadic activity is well represented by the equation:

$$\Delta N_{\rm spo} = 60 + 25\ sin(H + 4^h) \qquad (23)$$

with a minimum 2^h after local Noon. Hence, the difference between summer and winter seasons is most apparent in the nighttime rates and less so for the daytime rates.

Fig. 9 shows that $\Delta N_{\rm spo}$ and $< N_{\rm spo} >$ are out of phase, with $\Delta N_{\rm spo}$ peaking when $< N_{\rm spo} >$ changes most rapidly. To first order, $\Delta N_{\rm spo}$ follows a day-night cycle, while $< N_{\rm spo} >$ follows changes in the altitude of the Earth's apex. ΔN_{spo} is sensitive to the choise of the sporadic background level in September, a discussion of which is postponed until Sect. 6.

5.2. Meteor stream activity

After subtraction of the sporadic background, which varies as a function of time-of-day, we can increase the sensitivity for the detection of a meteor stream by adding the counts during the time that the stream radiant is above the horizon. Fig. 10 shows the average of counts over periods of 6 hours chosen to represent showers with radiants near the apex, the antapex, in Sun and anti-Sun directions. From these plots some 45 periodic enhancements of rates have been identified that are present in both the 1994 and 1995 data.

The very good agreement between 1994 and 1995 data is proof of the concept of "annual" meteor activity: showers that do not vary in activity significantly from year to year.

The occasional outbursts stand out strongly and are marked by an asterisk (*). Seven meteor outbursts were detected in 1994 and 1995: the 1994 and 1995 Perseid outbursts, the 1994 and 1995 Leonids (Jenniskens 1996a,b), the 1994 Ursids, the 1994 Aurigids (Jenniskens 1997) and the 1995 α-Monocerotids (Jenniskens et al. 1997).

The duration of the annual showers, the time of maximum activity and the peak rate after correction for observability are derived as follows. We assume that the activity curve of each meteor stream at time H has a profile (Jenniskens 1994):

$$N(H) = N(H)_{\rm max}\ 10^{B|\lambda_\odot - \lambda_\odot^{\rm max}|} \qquad (24)$$

Table 2. Model of meteor stream activity that fits the observed hourly and annual variation of meteor rates. Uncertain components are between brackets. The meteor streams are identified from: [1] Jenniskens (1994); [2] Sekanina (1976); [3] Cook (1973); [4] Kashcheyev & Lebedinets (1967); [5] Sekanina (1973). Note: *) Complex of streams.

#	Date (1995)	$\lambda_\odot^{max}$ (B1950)	B $^o)^{-1}$	RHR_{max} hr^{-1}	RA,DEC $\pm 15^o$		Identification	$<\lambda_\odot>$ ref.	RA,DEC reference	V_∞ ref.		χ [1]	ZHR_{max} hr^{-1}
1	Jan 04	282.59	2.5/0.37	2000	210,+40	Boo	Bootids	282.6	230,+49	43	[1]	2.5	140
2	Jan 06	285.1 ±0.5	0.20±0.05	300	090,+50	zAu	ζ Aurigids*	293.2	084,+58	16	[2]	-	5
3	Jan 12	290.4 ±0.7	0.20±0.05	280	230,+40	CBr	Corona-Borealids*	294.2	233,+37	37	[2]	-	15
4	Jan 19	298.2 ±0.5	0.20±0.05	310	120,+50	dCa	δ Cancrids*	296.4	130,+20	28	[2]	-	11
5	Jan 29	308.3±0.07	0.10±0.03	190	150,+10	aLe	α Leonids*	310.7	159,+06	29	[2]	-	7
6	Feb 08	317.7±0.5	0.20±0.05	100	170,+10	-	Febr. Draconids?	318.9	260,+74	23	[2]	-	3
7	Feb 16	325.0±0.5	0.20±0.05	80	180,+20	dLe	δ Leonids	330.7	154, +18	21	[5]	3.0	2
8	Feb 23	333.5±1.0	0.05±0.02	(200)	(120,–10)	-	δ Leonids?	338	159 +19	23	[1]	-	(6)
9	Mar 05	343.2±0.7	0.10±0.03	50	150,+10	pVi	π Virginids*	347.9	184,+01	32	[2]	3.0	2
10	Mar 21	359.0±1.0	0.05±0.02	100	170,+0	SVi	S-Virginids*	355.3	196,–01	28	[2]	3.0	4
11	Apr 04	013.0±1.0	0.05±0.02	70	250,+0	NVi	N-Viriginds*	011.9	210,–08	30	[2]	3.0	3
12	Apr 23	031.65	0.7/0.1	170	270,+30	Lyr	Lyrids	031.4	271,+32	49	[1]	2.7	13
13	May 04	043.1±0.5	0.3±0.05	1200	340,–20	eAq	η Aquarids	046	338,–01	66	[1]	2.7	(75)
14	May 07	045.8±0.8	0.08±0.01	500	350,+0	eAq	η Aquarids	046	338,–01	66	[1]	2.7	30
15	May 15	053.5±1.0	0.10±0.03	200	040,+10	MAr	May Arietids	054.3	037,+18	27	[2]	-	7
16	May 18	056±1	0.2±0.1	(300)	(130,–30)	-	-	-	-	-		-	(12)
17	May 26	064±2	0.08±0.01	(140)	(30,–20)	oCe	o Cetids	066.1	030,+01	35	[5]	-	(7)
18	Jun 07	075.2±0.3	0.10	330	060,+20	Ari	Arietids	076.9	039,+24	38	[1]	2.7	19
19	Jun 10	078.1±0.5	0.05±0.02	500	050,+30	zPe	ζ Perseids	070.5	063,+27	27	[2]	-	17
20	Jun 22	090.0±0.5	0.05±0.02	280	060,+30	-	α Draconids?	090.5	207,+64	19	[2]	-	6
21	Jun 26	093.9±0.5	0.3±0.05	(300)	(350,–20)	-	-	-	-	-		-	(12)
22	Jun 29	096±1	0.08±0.02	560	060,+30	bTa	β Taurids*	096	086,+19	30	[4]	-	20
23	Jul 04	102±1	0.07±0.01	70	310,+0	-	- *	-	-	-		-	3
24	Jul 09	106.4±0.5	0.20±0.05	400	340,–20	-	τ Capricornids?	109.5	311,–15	29	[2]	-	(15)
25	Jul 20	116.7±0.8	0.09±0.03	190	280,+60	-	o Draconids*?	117	098,+16	40	[4]	2.7	12
26	Jul 21	118.2±0.8	0.07±0.03	110	290,+20	Cap	α Capricornids*	126	305,–09	25	[1]	2.0	5
27	Jul 31	127.5±1.0	0.08±0.01	1000	360,–10	dAq	δ Aquarids	124.9	342,–16	42	[1]	3.3	(60)
28	Aug 08	135.4±0.3	0.30±0.05	200	090,+10	-	β Cepheids?	137.9	318,+73	28	[2]	-	7
29	Aug 13	139.44	0.22/0.05	1250	040,+60	Per	Perseids	139.4	042,+57	61	[1]	2.5	100
30	Aug 29	155.4±0.7	0.08±0.02	(300)	(40,–20)	mAr	μ Arietids	198	042,+20	43	[4]	-	(20)
31	Sep 08	167.0±0.5	0.10±0.05	(130)	(28,–20)	oPi	o Piscids	195	027,+09	31	[4]	-	(5)
32	Sep 30	186±2	0.08±0.02	200	150,+0	Sex	Sextantids	183.6	152,+0	32	[3]	-	9
33	Oct 14	201±5	0.03±0.02	90	010,+10	SAr	Southern Arietids	197.8	032,+10	28	[2]	-	3
34	Oct 22	207.9	0.12	500	090,–10	Ori	Orionids	208	094,+16	67	[1]	3.1	(30)
35	Nov 05	222.5±0.7	0.10±0.05	30	350,+0	eUm	Draconids-Ursids	223.4	261,+78	30	[2]	-	1
36	Nov 06	222.9	0.026	125	030,+10	Tau	Taurids	228.9	046,+17	30	[1]	2.3	6
37	Nov 11	229.2±0.5	0.20±0.05	200	050,+60	-	-	-	-	-		-	8
38	Nov 18	234.9	0.39	190	180,+20	Leo	Leonids	234.9	152,+22	71	[1]	3.0	(6)
39	Nov 20	236.6±0.5	0.20±0.05	240	060,+30	-	-	-	-	-		-	9
40	Nov 27	244.4±0.5	0.20±0.05	190	020,+60	-	-	-	-	-		-	7
41	Dec 01	248.8±0.5	0.12±0.03	280	060,+50	-	χ Orionids?	250.9	082,+23	28	[2]	-	10
42	Dec 14	261.4	0.70/0.09	2000	100,+40	Gem	Geminids	261.4	113,+32	36	[1]	2.6	110
43	Dec 18	265.4±0.5	0.20±0.05	220	220,+40	-	-	-	-	-		-	9
44	Dec 19	268.5±0.5	0.20±0.05	120	130,+40	-	Coma Berenicids?	262	156,+25	65	[3]	-	8
45	Dec 23	270.3	0.61	(100)	(320,+70)	Urs	Ursids	270.3	217,+75	35	[1]	3.4	(4)

Notes

2 Complex of two streams (Sekanina 1976 - [2]): ζ Aurigids which have $\lambda_\odot$ = 293.2 (B1950); RA,DEC = 84,+58; and V_∞ = 16 km/s, or in short: (293.2; 84,+58; 16), and the β Triangulids (286.7; 31,+33; 14). Also [5]: ρ Geminids (287.0; 109,+32; 22).

3 Complex of four streams [2]: January Bootids (294.2; 226,+44; 31), θ Corona-Borealids (294.5; 232,+31; 37), λ Bootids (294.5; 218,+44; 42), and Corona Borealids (294.6; 233,+35; 41).

4 Complex of three streams [2]: δ Cancrids (296.4; 130,+20; 28.4), January Cancrids (300.2; 125.1,+24.9; 23.5), and ψ Leonids (303.2; 143.2,+16.9; 30.4).

Table 2. (continued)

5 Complex of [2]: α Leonids (310.7; 159,+6; 29) and δ Leonids (313.8; 135,+8; 24).
6 Or radiant (335,+70). Could be another component of α Leonids.
7 Sekanina (1973) gives δ Leonids (330.7; 154,+18; 21). Data gap in [2].
8 σ Leonids (337.1; 169,+14; 25) in Sekanina (1973). Data gap in [2].
9 Complex of [2]: ρ Leonids (342.3; 161,+7; 24) and π Virginids (347.9; 184,+1; 32).
10 Complex of four streams [2]: Northern η Virginids (349.3; 182,+14; 26), Leonids-Virginids (349.5; 167,+28.1; 18); Southern η Virginids (170.4; 175,-2; 25); and Southern Virginids (355.3; 196,-1; 28). Also complex of Southern Virginids (3.7; 197,-7; 29) and Northern Virginids (359.5; 202,-3; 30) in [5]. Cook (1973) gives general "Virginids".
11 Complex of [2]: Northern Virginids (11.9; 211,-8; 30), α Virginids (18.4; 204,-12; 25) and Librids (15.2; 224,-13; 28). Perhaps contribution from κ Serpentids (14; 230,+18; 46) [3].
13 Is this a component of the η Aquarid shower? Profile seems to consist of a narrow and broad component.
15 Kashcheyev & Lebedinets (1967 -[4]) give shower at (54; 41,+23; 27).
17 Perhaps includes [2]: May-Ursids (58.9; 233,+76; 18).
18 [4] gives Arietids at: (77; 43,+23; 39).
19 [4] gives ζ Perseids at (71; 52,+23; 30).
20 Radiant can also be at (290,+60)
21 Perhaps components of [2]: σ Capricornids (92.3; 292,-14; 26) and θ Aurigids (95.3; 93,+31; 19).
22 According to Sekanina (1976) the β Taurids peak on July 4.4 (102.0). Includes component of [2]: Taurids-Arietids (98.6; 53,+22; 33). But Sekanina (1973) gives β-Taurids at (94.5; 79,+21; 28).
23 Radiant can also be at (190,+60). Possibly complex of 5-6 streams in Draco and Cepheus [2].
25 Radiant can also be at (90,+20). Perhaps also components of streams number 23 and 25 of reference [4].
26 Radiant can also be at (120,+60). Falls in gap of data in [2].
28 Radiant can also be at (290,+60).
31 "Southern Taurids" of Kashcheyev & Lebedinets (1967).
32 Stream numbers 32 and 37 to 40: Data gap in [2].
35 Radiant can also be at (230,+60).
41 Sekanina (1976) gives σ Taurids (250.9; 82,+23; 28) and μ Geminids (254.6; 94,+22; 31). χ Orionids are given at (257.5; 82,+23; 25). Sekanina (1973) gives "Monocerotids" (243.7; 91,+15; 42).

The equation has three free parameters for each shower: the peak activity $N(H)_{\rm max}$, the time of maximum $\lambda_{\odot}^{max}$ and the equivalent duration of the shower (Jenniskens 1994):

$$\Delta T = 0.881/B \qquad \text{days} \tag{25}$$

whereby the duration is expressed in the parameter B here. All peaks are fitted with Eq. 24, until the sum of all profiles provides a fit to the data by adjusting $N(H)_{\rm max}$, B, and $\lambda_{\odot}^{\rm max}$.

In order to simplify the analysis slightly, we adopt for the major streams the shape of the activity curve as derived from visual observations, adopting B and $\lambda_{\odot}^{\rm max}$ from Jenniskens (1994). These include the Quadrantids, Lyrids, η Aquarids, Arietids, Perseids, Orionids, Taurids, Leonids, Geminids, and Ursids. In all cases, these profiles produce good fits to the radio data, except for the η Aquarids. That shower seems to have an additional sharp component centered at solar longitude 43.1 which is listed as a separate stream in Table 2. We suspect a a meteor outburst such as the 1993 Orionid outburst (Jenniskens 1995), discussion of which is postponed.

The "minimalistic" approach was taken: if a single stream can fit a peak in another time interval, no new stream is postulated. In three occasions, the total sum does not match the observed rates and the existence of an additional (broad and shallow) stream is introduced to the model in order to provide a good fit. These streams are not identified from peaks in the reflection count distribution: the May 26 ($\lambda_{\odot}$ = 64) stream, the Sept. 8 (167) stream, and the October 14 (201) stream. However, all three are identified with known dispersed streams.

The fitting procedure is first applied to the sum of all data in the six-hour intervals shown in Fig. 10, in order to have highest signal-to-noise. Then the resulting sample of streams is used to fit all 24 curves of 1-hour interval data (e.g. Fig. 8), giving $N(H)_{\rm max}$ for all hours H. That variation of rates during the day (e.g. Fig. 5) is used to find the radiant (RA,DEC) of the meteor stream, from a comparison with the observability function of Fig. 4.

Once the declination of the stream has been derived, the peak rate $N(H)_{\rm max}$ is corrected with the peak observability at that declination (Fig. 4). The corrected peak Radio zenith Hourly Rates ($RHR_{\rm max}$) and the radiant position are listed in Table 2.

There are some pitfalls to our method of analysis of which the reader should be aware. There is ambiguity between low and high declination (> 60 degree) radiants, which give a similar rate evolution, but with a significantly different time of minimum activity. Hence, the right ascension of the radiant can be far off if the declination is chosen in the wrong regime (such alternatives are given in the notes to Table 2). The method also assumes that each peak in the activity curve is due to only one meteor stream. In fact, several peaks are suspected to be the result of a multitude of streams, based on the radar orbit catalogues (marked by an asterix in Table 2). Peaks that are present at various local hours may be due to unrelated streams that peak at different times in the day but at about the same day of the year. Only if the

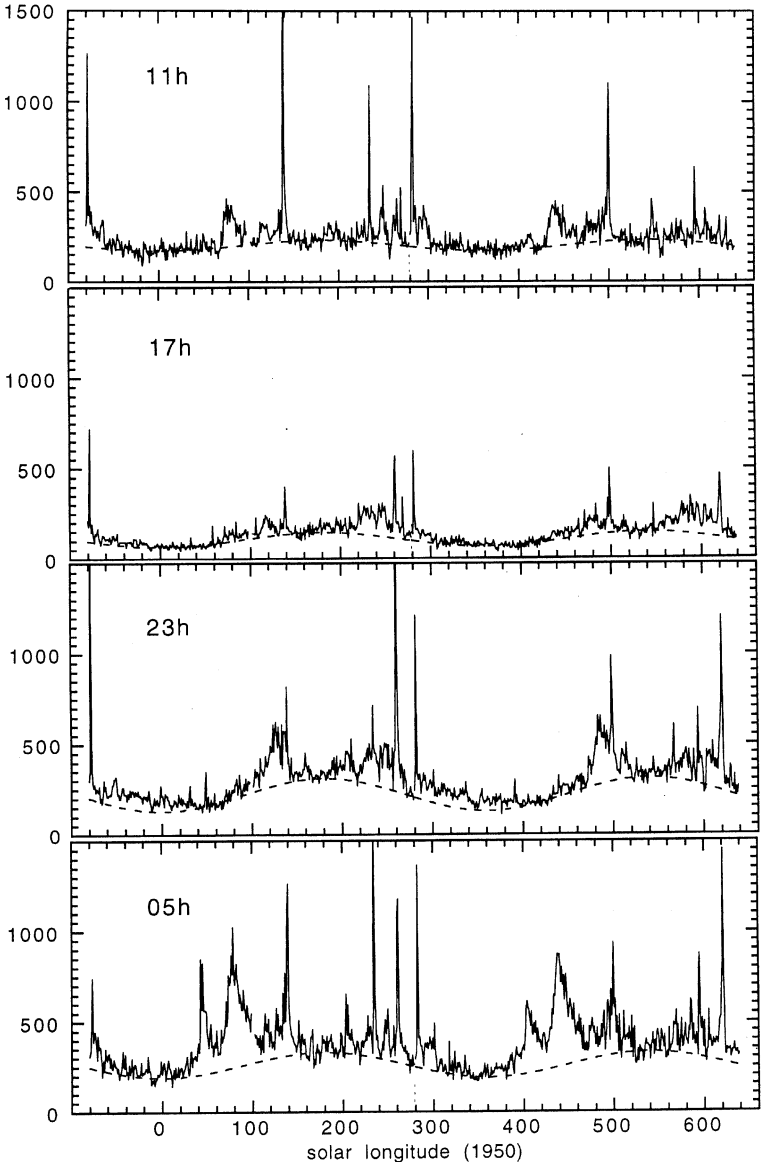

Fig. 8. Hourly count of meteor reflections at four characteristic times of the day (in UT). A dashed line gives our choice of the sporadic background baseline. All features above that line are due to meteor streams.

radiants are in a similar part of the sky does a correct stream identification follow. Only in that case is the correction of peak rates for observability correct. Further observations are needed to eliminate these uncertainties.

There is reason to assume that in most cases we arrived at the correct answer. We compared our radiant positions and times of maximum activity to the catalogs of meteor streams compiled by Sekanina (1973) and Sekanina (1976) from the Radio Meteor Project (with limiting magnitude +11) and the radar orbit catalog of Kashcheyev & Lebedinets (1967). Although the catalogs are not complete, as many as thirty enhancements can be identified with known meteor streams, another eight doubtfully. Those peaks that seem to be caused by a number of streams in the existing catalogues are mentioned in the notes to Table 2.

We find that all streams with a relatively large number of meteoroids in the radar surveys are also recognized in our meteor rate survey. Three showers that perhaps should have been detected are the Soutern ι Aquarids, placed at August 10 ($\lambda_\odot$ = 137.3; RA = 343, DEC = -3; V_∞ = 27 km/s) by Sekanina (1976), the Piscids (172.8; 09,+07; 27.8 km/s) on Sept. 16, and a group of Cameleopardalid showers (182.2; 104,+77; 34 km/s) on Sept. 26. The first stream is confused by the Perseid shower but may contribute to an unidentified peak on August 8. The Piscids and Cameleopardalids are dispersed streams and active in September and may have been included in the sporadic background incorrectly here. We have not corrected for this, because we do not apriori know at what level to place the sporadic background.

The radio rates RHR_{max} can be used to calculate meteor stream influx by scaling to Zenith Hourly Rates (ZHR):

$$ZHR_{\max} = RHR_{\max}\, C(A_{\rm eff})\, C(\chi)\, \chi^{(6.5-{\rm Lm})} \qquad (26)$$

and using equations given in Jenniskens (1994). Note that approximately the same magnitude interval is considered and we can safely use χ as derived from visual observations. In this formula, $C(A_{eff})$ is the ratio of effective surface areas sampled between the visual and radio techniques, while $C(\chi)$ accounts

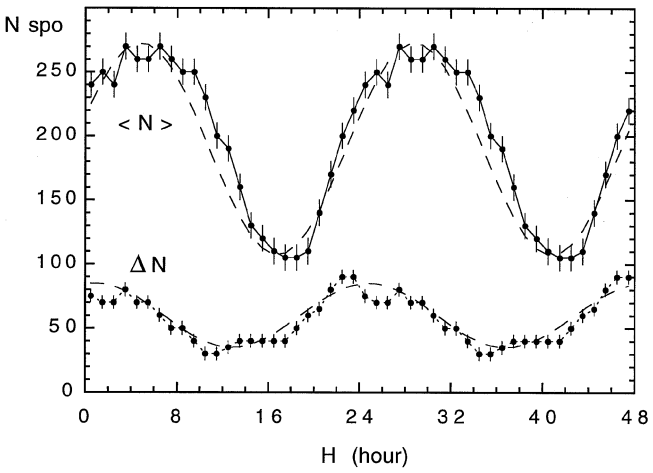

Fig. 9. Daily variation of sporadic rates. The yearly mean of sporadic rates at a given time of day $< N_{\rm spo} >$ (upper curve) is shown alongside the amplitude of the seasonal variation $\Delta N_{\rm spo}$ at that hour of the day (lower curve).

for the increase of counts due to multiple counted overdense echoes. For many streams the parameter χ remains unknown. When necessary, we used adopted values of χ = 3.0 and V_∞ = 30 km/s.

The effective surface area for the MS system as compared to that for a standard visual observer was derived by comparing the detected sporadic rates, and found to be about 4.4×10^{11} m^2. That is about 40% of the potential reflection surface at 100 km altitude (Verbeeck 1995). The effective surface area observed by a standard visual observer is a function of meteor velocity (Jenniskens 1994) and the correction becomes:

$$C(A_{\rm eff}) = 0.052 + 0.0017\ V_\infty \quad (27)$$

Overdense echoes are counted a fraction of about 2.3 too often on average, or even more when the magnitude distribution index is less than 2.5. We find that C(χ) is about 0.8 for sporadic meteors, about 0.4-0.7 during the Perseids and can be much lower when a stream is rich in bright meteors. We have adopted:

$$C(\chi) = 0.86 + 0.0155\ V_\infty - 0.00037\ V_\infty^2 \quad (28)$$

but note that a much less strong correction such as:

$$C(\chi) = 1.04 - 0.0039\ V_\infty - 0.000037\ V_\infty^2 \quad (29)$$

gives much the same result for all but the fastest showers.

Comparing the measured radio zenith hourly rate $\rm RHR_{max}$ and the visual zenith hourly rate $\rm ZHR_{max}$ for the streams in Table 1, after correction for C($\rm A_{eff}$) and C(χ), results in an effective limiting magnitude Lm defined by Eq. 26. These results are shown by dark symbols in Fig. 3, both for Eq. 28 (large symbols) as for Eq. 29 (small symbols).

In both cases, the limiting magnitude is much less strong a function of V_∞ than suggested by the classical radio echo model (open symbols). From Fig. 3, we find for our system:

$$Lm = 8.4 - 0.034\ V_\infty \quad (30)$$

It is not clear to us why the sensitivity is so much less dependent on entry velocity than predicted in the classical model.

Eqs. 26, 27, 28, and 30 are used to scale $\rm RHR_{max}$ to the equivalent $\rm ZHR_{max}$ (Table 2). No error estimates are given, but we expect the result to be within a factor of three to the true value. Least certain values are given between brackets, notably those with low radiant declination and high entry velocity.

6. Discussion

6.1. The sporadic rates

The diurnal variation of meteor rates has been studied by many (e.g. Lovell 1954, Hines 1956, Hawkins 1956, Meeks & Jones 1959, Keay 1963, Hughes 1990). In spite of that, the diurnal variation of sporadic meteor rates has remained elusive, mainly because of the presence of (unrecognized) stream activity in the data (Hughes 1990). Recent studies have modelled theoretical distributions of meteor radiants to the data (e.g. Mawrey & Broadhurst 1993, Weitzen 1986), but these are very poor representations of the real distribution of meteors in space.

Our results confirm that the relative contribution of the Sun component in the distribution of radiants, peaking at ecliptic coordinates L = 342, B = +0, and the anti-Sun component, peaking at L = 198, B = +1, (e.g. Elford 1967, Jones & Brown 1993, 1994) is significantly diminished when the known meteor streams are excluded from the sample (Elford 1967).

More interesting perhaps is the amplitude of the annual variation of sporadic rates, a topic that is debated (Mawrey & Broadhurst 1993). The open question is if the density of sporadic meteoroids is higher in the second half of the year as opposed to the first half (e.g. McKinley 1961).

We do find a seasonal variation (Fig. 9), with a somewhat time-of-day dependent amplitude. At first sight, it appears as if the daytime rates are increased by about 25%, which causes a decrease of the summer/autumn variation (Fig. 9). It is hard to understand how this can happen. It cannot be an effect of the Sun's presence in the antenna beam, because that would suggest a more serious effect in winter. Galactic noise is also not a likely cause because the antenna pattern does not have sharp minimas, except at the zenith, and the front/back ratio is only 6 dB. Similarly, the day to nighttime difference in D-layer absorption (at 81 km altitude), or E-layer absorption (at 105 km) (Vogan & Campbell 1957), is negligible at VHF frequencies, for which we calculated that counts may be affected by 0.5% at most. Also polarization rotation losses cannot acount for the effect. Rotation of the polarization plane occurs during scattering of the wave by the train and by ionospheric Faraday rotation. The polarization rotation losses vary as a function of local time, peaking two hours after local noon (Baggaley 1979, Cannon 1985). That mimicks the observed decrease of the daily variation of the seasonal amplitude (Fig. 9), but is not accompanied by a decrease of the mean rates during daytime. Indeed, the effect is not strong at 87 MHz. Cannon (1985) reported a daily mean loss of 50% at 40 MHz, decreasing rapidly with increasing frequency. At 87 MHz, we detected only 12% of counts with

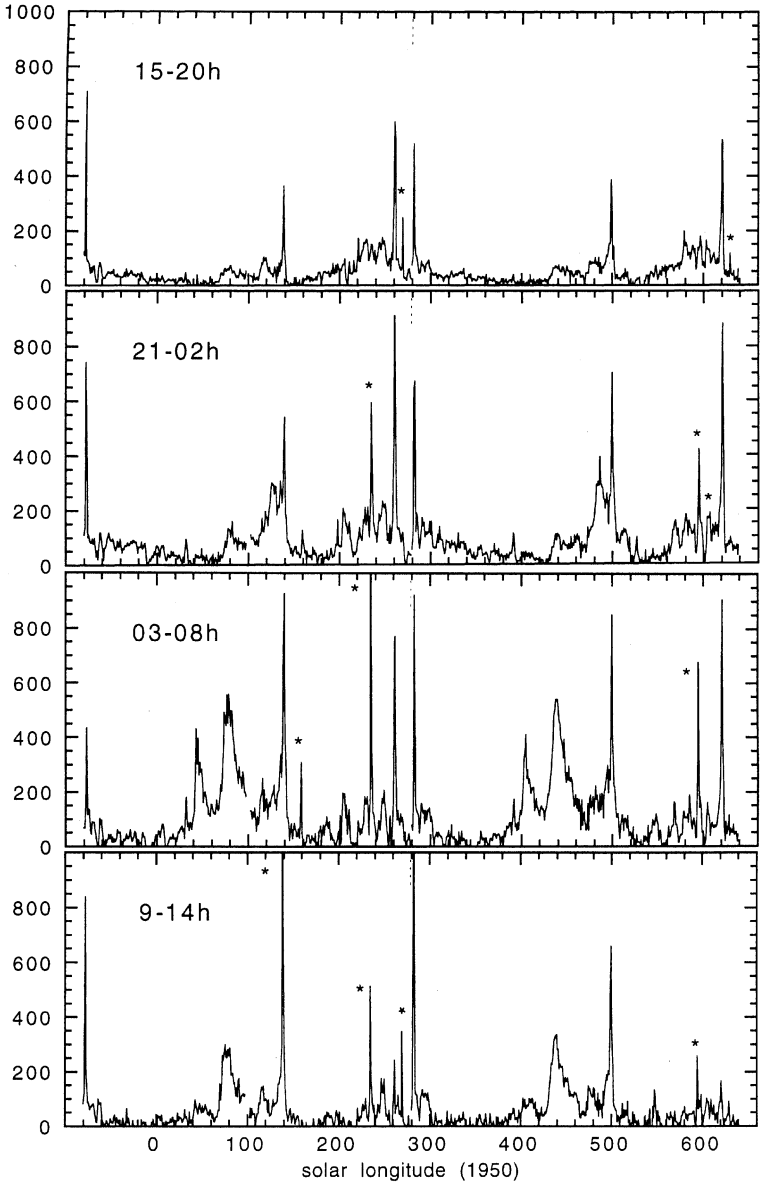

Fig. 10. Meteor rates after subtraction of the sporadic background. Mean values are given for the periods in UT that are indicated.

a horizontally polarized antenna, suggesting that polarization losses can account for at most N = 15-30 per hour.

Instead, we believe that the observed effect is as benign a thing as unrecognized minor streams contributing to the evening and nighttime September data. Indeed, the catalog of radar orbits by Sekanina (1976) lists a number of dispersed Piscid and Cameliopardalid showers that month, which together could contribute some N = 50 per hour to the total rate. In that case, the remaining seasonal amplitude is only ± 40 per hour and would be constant over the time of day. That seasonal amplitude is probably fully accounted for by the varying altitude of the apex in various seasons at a given time of the day.

Alternatively, some amount of the remaining seasonal variation may reflect daily variations in the atmospheric scale height, as a result of which the diffusion timescale of the meteor trails varies (Hughes 1976). The variation is of order 30% and consistent with daily variations of order 20-25% reported by Lindblad (1978). Such variations also affect the meteor stream rates and may contribute to the value of the exponent γ in the radiant altitude correction of visual rates (Jenniskens 1994).

6.2. Meteor stream activity

The results of Table 2 complete earlier surveys of meteor stream activity of visual night-time annual streams (Jenniskens 1994). Not included yet are southern hemisphere daylight showers. There is also some bias in favor of dispersed streams with intermediate entry velocity.

The meteor streams in our sample tend to be broader on average than in the visual sample of Jenniskens (1994) and contain a larger fraction of dispersed ecliptic showers. Showers with extreme velocities (either very fast or very slow) are less abundant than in the night time visual stream sample.

The absence of minor streams of fast meteors may reflect an echo height ceiling, but we saw that the effect is less strong than expected based on the classical radio echo theory. More likely, the current list of visual streams over-represents streams that stand out from the sporadic background, i.e. which have relatively high or low entry velocity and which are of short duration.

7. Conclusions

It has been demonstrated that an automatic meteor counting system using forward meteor scatter can be built stable enough to produce similar counts in two successive years. From the present data as many as 45 annual meteor streams can be recognized, some of which have peak rates as low as ZHR = 3-4 meteors per hour. We find that our system detects meteor streams of high entry velocity with much higher relative sensitivity than suggested by the classical radio echo theory.

Meteor streams are found on top of a continuous background, defined as the sporadic activity. The diurnal variation of this background is well described by a homogeneous distribution of radiants, with a mean heliocentric velocity of $< V_H >$ = 36 km/s (or $< V_\infty >$ = 41 km/s). We confirm that once the meteor streams are extracted from the data, Sun and anti-Sun components are of relatively minor importance among large meteoroids. The amplitude of the seasonal variation is sinusoidal. Allowing for some uncertainty in the September stream contribution, we find that the seasonal amplitude is only 20% or less and constant for different times of the day. However, for a given choise of the sporadic background in September, we find a weak time-of-day dependence, with the smallest variation of the seasonal amplitude two hours after local noon.

Forty-five enhancements of meteor rates are detected, 30 of which are identified with known meteor streams from radar orbit catalogs. At least 10 are due to multiple dispersed streams. All streams that stand out in the radar data (at a limiting magnitude +11) are detected also in our meteor rate survey with a typical sensitivity of +7, with the exception of streams that are confused by more active ones. Many are minor nighttime streams that are not conspicuous in visual observations, either because of a velocity similar to sporadic meteors or because they are very dispersed. The data also cover daylight meteor showers down to the detection level of nighttime showers. The equivalent peak Zenith Hourly Rate, the stream duration, and time of maximum have been calculated, which add to similar results derived from visual observations. These parameters further refine models of the near-Earth dust environment.

The results presented here will serve as a basis for further employment of this and similar systems in a recently established Global Meteor Scatter Network (Global-MS-Net), aimed at detecting meteor outbursts by a continuous monitoring of the level of meteor activity (Jenniskens et al. 1997a). Further information on Global-MS-Net can be found at: http://www-space.arc.nasa.gov/∼leonid/GlobalMSNet.html

Acknowledgements. We thank Thomas Volguards of DTe Mobil for information concerning the Eurosignal network. The paper benefited from comments by referee David Hughes. The present analysis of the radio meteor scatter data was made possible by grants from the NASA/Ames Research Center Director's Discretionary Fund and NASA's Research in Planetary Astronomy and Planetary Atmospheres program. PJ is associated with the SETI Institute.

References

Artoos D., 1990, WGN, Journal of IMO 18, 101
Baggaley W.J., 1979, J. Atmos. Terr. Phys. 41, 671
Bus E.P., 1995, Radiant, Journal of DMS 17, 43
Cannon P.S., 1985, Polarisation Rotation in Meteor Burst Communication Systems, Royal Aircraft Establishment Technical Report 85082.
Cannon P.S., Reed A.P.C., 1987, J.-IERE 57, 101-112
Cook A.F., 1973, in Evolutionary and Physical Properties of Meteoroids, NASA SP-319, Washington D.C., 183
Elford W.G., 1967, Smits. Cont. Ap 11, 121
Eshleman V.R., Manning L.A., 1954, Proc. Inst. Radio Engrs. 42, 530
Forsyth P.A., Hines C.O., Vogan E.L., 1955, Can. J. Phys. 33, 600
Hawkins G.S., 1956, MNRAS 116, 92
Hawkins G.S., 1964, Ann. Rev. Astron. Astrophys. 2, 149
Hawkins G.S., Aspinall A., 1954, in Meteor Astronomy, by A.C.B. Lovell, Oxford Clarendon Press, p. 391
Hey J.S., Stewart G.S., 1946, Nature 158, 481
Hines C.O., 1955, Can. Journ. Phys. 33, 493-503
Hines C.O., 1956, J. Atm. Terr. Phys. 9, 229
Hines C.O., Vogan E.L., 1957, Can. Journ. Phys. 35, 703
Hughes D.W., 1976, Space Research 16, 333
Hughes D.W., 1982, Vistas in Astronomy 26, 325
Hughes D.W., 1990, MNRAS 245, 198
Jenniskens P., 1994, A& A 287, 909
Jenniskens P., 1995, A& A 295, 206
Jenniskens P., 1996a, Meteoritics & Planetary Sci 31, 174
Jenniskens P., 1996b, WGN, Journal of IMO 23, 198
Jenniskens P., 1997, A& A 317, 953
Jenniskens P., Betlem H., de Lignie M., Langbroek M., 1997, ApJ 479, 441
Jenniskens P., Yrjölä I., Sears P., Kuneth W., Rice T., 1997a, WGN, Journal of IMO 25, 141
Jones J., Brown P., 1993, MNRAS 265, 524
Jones J., Brown P., 1994, Planet. Space Sci. 42, 123
Kashcheyev B.L., Lebedinets V.N., 1967, Smits. Cont. to Ap. 11, 183
Keay C.S.L., 1963, MNRAS 126, 165
Kresáková M., 1966, Contr. Ast. Obs. Skalnate Pleso 3, 75
Kristensen G.M., 1991, WGN, Journal of IMO 19, 206
Lehtoranta V.K., 1987, Radiant, Journal of DMS 9, 101
Lindblad B.A., 1978, Nature 273, 732
Lovell A.C.B., 1954, Meteor Astronomy, Oxford Clarendon Press, pp. 463
Manley T.R., 1990, WGN, Journal of IMO 18, 163
Mason J., 1986, J. Britt. Astron. Assoc. 96, 118
Mawrey R.S., Broadhurst A.D., 1993, Radio Science 28, 428
McKinley D.W.R., 1961, Meteor Science and Engineering, McGraw-Hill, New York, Ch. 8 and 9, 309pp.
Meeks M.L., James J.C., 1959, J. Atmos. Terr. Phys. 16, 228
de Meyere M., Steyaert C., 1984, Werkgroepnieuws, Journal of the VVS Section on Meteors 12, 171
Millman P.M., McKinley D.W.R., 1956, Can. J. Phys. 34, 50
Moorcroft D.R., Hines C.O., 1958, Can. J. Phys. 36, 134
Morrow M.J., Moore B.R., 1990, WGN, Journal of IMO 18, 90

Pierce J.A., 1938, Proc. Inst. Radio Engrs., 26, 892
Pilon K.V., 1984, Meteoros, Journal of the BMS 14, 10
Prentice J.P.M., Lovell A.C.B., Banwell C.J., 1947, MNRAS 107,155
Ralston W.T., Weitzen J.A., Ostergaard J.C., 1993, Radio Science 28, 747
Richardson J., 1995, WGN, Journal of IMO 23, 56
Schiaparelli G.V., 1866, Note e Riflessioni sulla theoria astronomica delle stelle candenti
Schilling D.L., 1993, Meteor Burst Communications (Theory and Practice), Wiley Series in Communication
Sekanina Z., 1973, Icarus 18, 253
Sekanina Z., 1976, Icarus 27, 265
Shimoda C., Suzuki K., Maeda K., 1993, WGN, Journal of IMO 21, 130
Steel D., 1993, in Asteroids Comets Meteors 1993, IAU-Symp. 160, A. Milani, M. Di Martino, A. Cellino (eds.), Kluwer, p. 111
Steyaert C., 1987, WGN, Journal of IMO 15, 193
Sugar G.R., 1964, Proc. IEEE 53, 117
Suzuki K., Nakamura T., 1995, WGN, Journal of IMO 23, 17
Tepliczky I., Spanyi P., 1991, WGN, Journal of IMO 19, 216
Verbeeck C., 1995, WGN, Journal of IMO 23, 236
Vogan E.L., Campbell L.L., 1957, Can. J. Phys. 35, 1176
van Wassenhove J., 1987, WGN, Journal of IMO 15, 116
Weitzen J.A., 1986, Radio Science 21, 1009
Weitzen J.A., Ralston W.T., 1988, IEEE Trans. on Antennas and Propagation 36, 1813
Weitzen J.A., Cannon P.S., Ostergaard J.C., Rasmussen J.E., 1993, Radio Science 28, 213
White R., 1995, WGN, Journal of IMO 23, 62

This article was processed by the author using Springer-Verlag LaTeX A&A style file L-AA version 3.